American Journal of Modern Physics
2026, Vol. 15, No. 3, pp. 86–95
https://doi.org/10.11648/j.ajmp.20261503.13

SciencePG
Science Publishing Group

Research Article

Modeling of Coupled Heat and Mass Transfer for the Optimization of Evaporative Cooling Using a Porous Clay Plate

Salifou Cisse[1, *], Windnigda Zoungrana[1], Jacques Nébié[1, 2], Boureima Kaboré[1, 3], Nebyinga Béatrice Komi[1], Abdoul Aziz Ouiminga[1, 4], Sié Kam[1]

[1]Department of Physics, Joseph Ki-Zerbo University, Ouagadougou, Burkina Faso
[2]Department of Physics, Thomas Sankara University, Saaba, Burkina Faso
[3]Department of Physics, Norbert Zongo University, Koudougou, Burkina Faso
[4]Department of Physics, Ecole Normale Supérieure (ENS), Koudougou, Burkina Faso

Abstract

This study investigates the complex mechanisms of coupled heat and mass transfer within a fired porous clay plate optimized for evaporative cooling in hot and dry climates. The primary objective was to model and experimentally validate the material's ability to lower air temperature through capillary evaporation. Local results highlight a pronounced leading-edge effect, where a maximum evaporation flux of 0.78 g/m² induces rapid cooling within the first few centimeters of the plate. Under nominal conditions of 40°C and 20% relative humidity (RH), the outlet air temperature drops significantly to 25.38°C, corresponding to a thermal gain of nearly 15°C. The theoretical validity of the model is confirmed by the perfect superposition of local Nusselt (Nu_x) and Sherwood (Sh_x) numbers, demonstrating the consistency of the Chilton-Colburn analogy. Parametric analysis reveals that system efficiency is highly dependent on residence time and hygrometric potential: a moderate air velocity of 1.5 m/s combined with low initial humidity (10%) optimizes the process, achieving a record cooling of 17.4°C. Despite some simplifying assumptions (adiabatic walls, uniform saturation), comparison with experimental data shows excellent agreement, with an average relative error of 6% to 7% and a root mean square error (RMSE) of approximately 2°C. The research demonstrates that fired clay, owing to its porous structure that promotes capillary transport, constitutes an efficient passive heat exchanger and a sustainable alternative to energy-intensive air conditioning systems.

Keywords

Fired Clay, Porous Media, Water, Coupled Transfers (Heat and Mass), Saturation, Evaporation

*Correspondence: Salifou Cisse (shalcisde@gmail.com)

Received: 14 April 2026; **Accepted:** 27 April 2026; **Published:** 11 May 2026

1. Introduction

The study of coupled heat and mass transfer in unsaturated porous materials is of paramount importance for air cooling in hot and dry climates, as it enables the understanding and optimization of evaporative cooling processes, which rely on water evaporation [1, 2]. In hot and dry climates, ambient air exhibits high temperature and low relative humidity [3]. This condition creates a significant thermodynamic potential, as the air can absorb a large amount of water vapor before reaching saturation [4, 5]. The energy required for water evaporation—latent heat—is extracted from the hot and dry air, resulting in its cooling [6]. Water evaporation, involving mass transfer, leads to air cooling through heat transfer, thereby modifying its thermophysical properties [7]. Heat and mass transfer phenomena are inherently coupled in this process, which is essential for accurately evaluating thermal and energy performance [8, 9]. A thorough understanding of coupled heat and mass transfer allows for the design and optimization of eco-friendly and cost-effective cooling systems, such as direct and indirect evaporative coolers, desiccant air conditioning systems, or cooling towers [10, 11]. Evaporative cooling systems using porous plates offer several advantages over conventional air conditioners: they consume significantly less energy and use water as a natural refrigerant [12]. In countries with hot and dry climates, evaporative cooling can reduce air temperature by 10 to 20°C, providing a sustainable solution well-suited to energy and environmental constraints [12-14]. Mastering coupled heat and mass transfer in porous materials such as fired clay not only optimizes the efficiency of evaporative cooling systems but also enhances thermal comfort [12, 14]. The objective of this study is to develop a detailed model of coupled heat and mass transfer in a permanently water-saturated fired clay plate subjected to a stream of hot and dry air, in the context of an evaporative cooling system.

2. Materials and Methods

2.1. Materials Used

The base material considered is fired clay, obtained by firing natural clay at temperatures between 900 and 1100°C. This process imparts an open, interconnected porous structure that is particularly favorable for capillary transport and evaporation. Water serves as the evaporating fluid: it adsorbs within the porous structure of the clay, diffuses through the pores, and evaporates at the surface in contact with air. It migrates by capillarity to the outer surface, where it evaporates by absorbing thermal energy from the hot and dry air. Air is the fluid whose thermal and hygric properties are to be modified. The influencing parameters include dry-bulb temperature, relative humidity, flow velocity, and vapor pressure.

The physical properties of fired clay, air, and water are summarized in Table 1.

Table 1. *Physical properties of fired clay, air, and water [12-14].*

Properties	Cooked clay	Air
Thermal conductivity ($W.K^{-1}.m^{-1}$)	0.6	0.0275
Specific heat ($J.kg^{-1}.K^{-1}$)	850	1007
Volumic mass ($kg.m^{-3}$)	1380	1.15
Dynamic viscosity (Pa.s)	--	1.8×10^{-5}
Porosity (%)	0.45	--

2.2. System Configuration

The investigated system consists of a flat porous fired clay plate of thickness e, length L, and width w. The plate is permanently saturated with water through continuous supply (via capillary action or external feeding) and exposed on both sides to parallel flows of hot and dry air. The air streams flow along the plate surfaces, enabling coupled heat and mass transfer through evaporation. A schematic representation of the system is illustrated in Figure 1.

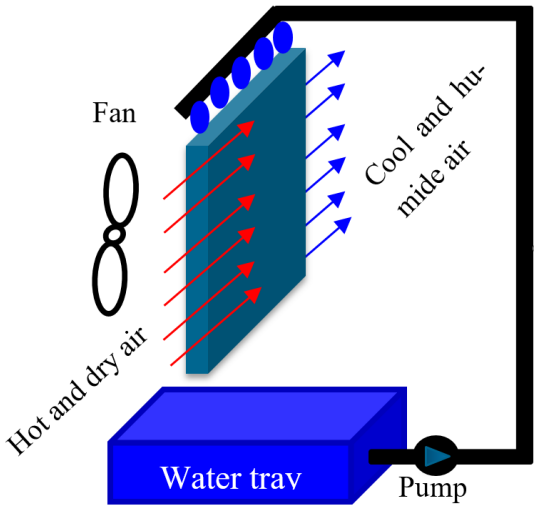

Figure 1. Schematic diagram of the system.

3. Modeling of Coupled Heat and Mass Transfer

3.1. Model Assumptions

For the modeling of coupled heat and mass transfer in fired clay, the following simplifying assumptions were adopted:

1) The air flow is steady-state and remains laminar.
2) The transfers are unidirectional.
3) The solid phase is non-deformable.
4) The fluid components of the porous medium are incompressible.
5) The boundary layer near the plate-dry air exchange surface is always saturated with water, and the vapor pressure corresponds to the saturation vapor pressure.
6) The Chilton-Colburn analogy between heat transfer and mass transfer is valid, allowing the use of identical forms of correlations for the Nusselt number and the Sherwood number, with the same dependence on the Reynolds number.
7) The plate is in adiabatic thermal equilibrium, meaning that the sensible heat flux received from the air is entirely consumed by the latent heat flux due to evaporation. Internal heat sources, thermal radiation, and thermal inertia of the support are neglected.
8) Gravity effects are assumed to be negligible.

The transfers at the plate surface are dominated by forced convection under laminar regime.

3.2. Modeling of Internal Transfers in the Porous Plate

Given that the plate is porous and continuously supplied with water, the general model of coupled heat and mass transfer is used. The objective is to simulate the movement of liquid water toward the surface to sustain evaporation.

3.2.1. Energy Balance – Heat Conservation in the Porous Plate

The heat transfer equation in the plate incorporates conduction and the latent heat term resulting from internal phase changes [15]. It is given by Equation (1).

$$(\rho C_P)_{eff} \frac{\partial T}{\partial t} = \nabla \cdot (\lambda_{eff} \nabla T) - \dot{m}_{phase} L_v \quad (1)$$

With:

λ_{eff}: Effective thermal conductivity of the medium which depends on the porosity ε and the water content (W/(m·K))

$\dot{m}_{phase}$: Mass rate of water vapor produced by evaporation per unit volume (kg/(m³·s)).

L_v is the latent heat of vaporization (J/kg).

$(\rho C_P)_{eff}$ is the effective volumetric heat capacity, given by Equation (2):

$$(\rho C_P)_{eff} = \left(\varepsilon \rho_f C_{P,f} + (1-\varepsilon)\rho_s C_{P,s}\right) \quad (2)$$

3.2.2. Mass Transport Equation in the Porous Plate

The mass transport equation in the plate relates the variation in vapor concentration to its diffusion and source/sink terms [16]. It is given by Equation (3):

$$\frac{\partial(\varepsilon \rho_v)}{\partial t} = \nabla \cdot D_{eff} \nabla \rho_v) - \dot{m}_{evap} \quad (3)$$

With:

D_{eff}: Effective diffusivity of vapor in the pores (depends on porosity and tortuosity).

$\dot{m}_{evap}$: This term ensures the coupling between the two equations. It represents the evaporation rate within the pores, which consumes heat and produces vapor.

3.3. Properties of Moist Air and Empirical Formulas

The saturation vapor pressure of water is used to calculate the saturated vapor density and relative humidity. The saturated vapor density is given by Equation (4):

$$\rho_{v,sat}(T) = 0.018015.\frac{P_{sat}(T)}{8.314T} \quad (4)$$

With:

$$P_{sat}(T) = 611.2exp\left(\frac{17.67(T-273.15)}{T-273.15+243.5}\right) \quad (5)$$

The relative humidity of air is given by Equation (6):

$$HR = \frac{\rho_{v,a}}{\rho_{v,sat(T)}} \quad (6)$$

3.4. Sensible Heat Balance Air–Water (Coupling)

The exchanges at the interface couple the thermodynamic equations of the air and the plate through evaporation.

The variation in air temperature expressing the evaporation rate $\dot{m}_{evap}$ through mass transfer is given by Equation (7) [17]:

$$\rho_{air}C_{p,air}\frac{dT_{air}}{dt} = \frac{Nu_{air-plaque}\cdot\lambda_{air}}{L}\left(T_{air,0} - T_{air,i}\right) + \dot{m}_{evap}L_v \quad (7)$$

The evaporation flux j_ev is given by Equation (8):

$$\dot{m}_{evap} = h_m \cdot (\rho_{v,surface} - \rho_{v,\infty}) \quad (8)$$

Where:

$\rho_{v,surface}$: Water vapor density at the surface (saturated).

$\rho_{v,\infty}$: Water vapor density in the free air stream.

h_m: Evaporation flux (kg/(m²·s)).

3.5. Convective Heat Transfer Coefficient

The convective heat transfer coefficient λ_{air} quantifies the ability of the air flow to exchange thermal energy with the surface. It is derived from the Nusselt number (Nu), a dimensionless number representing the ratio between convective and conductive heat transfer, and is given by Equation (9) [17]:

$$h_{air} = \frac{Nu\cdot\lambda_{air}}{L} \quad (9)$$

where:

λ_{air}: Convective heat transfer coefficient (W/(m²·K))

L: Characteristic length of the plate (m)

For laminar flow over a flat plate, the standard empirical correlation for the Nusselt number at the air-plate interface is given by Equation (10):

$$Nu_{air-plaque} = 0.453R_e^{0.5}.Pr^{1/3} \quad (10)$$

with:

$$R_e = \frac{V\times L}{v} \quad (11)$$

where:

V: Characteristic air velocity (m/s)

L: Characteristic length (m)

v: Kinematic viscosity of air (m²/s)

3.6. Convective Mass Transfer Coefficient

The convective mass transfer coefficient h_m is obtained using the Chilton-Colburn analogy. This analogy links heat transfer and mass transfer by exploiting the similarity of transport mechanisms in the boundary layer [18, 19]. It is given by Equation (12):

$$h_m = \frac{Sh\cdot D_{v,air}}{L} \quad (12)$$

where:

h_m: Convective mass transfer coefficient (m/s)

$D_{v,air}$: Diffusivity of water vapor in air (m²/s)

Sh: Sherwood number

The Sherwood number is given by Equation (13):

$$Sh = Nu \cdot \left(\frac{Sc}{Pr}\right)^{1/3} \quad (13)$$

where Sc is the Schmidt number and Pr is the Prandtl number.

3.7. Solution Method

The equations are solved iteratively using an explicit method with a simulation program developed in MATLAB software.

4. Results and Discussion

4.1. Evolution of the Evaporation Rate Along the Plate

Figure 2 shows the evolution of the local evaporation flux along a fired clay plate 20 cm in length.

The evaporation flux reaches a peak of 0.78 g/(m²·s) at the

inlet (x = 0), then drops by 80% within the first 5 cm before stabilizing near zero at x = 20 cm. This profile reflects the development of a diffusion boundary layer where the concentration gradient is maximal at the start. As air progresses, it becomes loaded with vapor and the layer in contact with the clay tends toward saturation [20]. Consequently, the majority of mass transfer and latent heat extraction is concentrated at the very beginning of the plate.

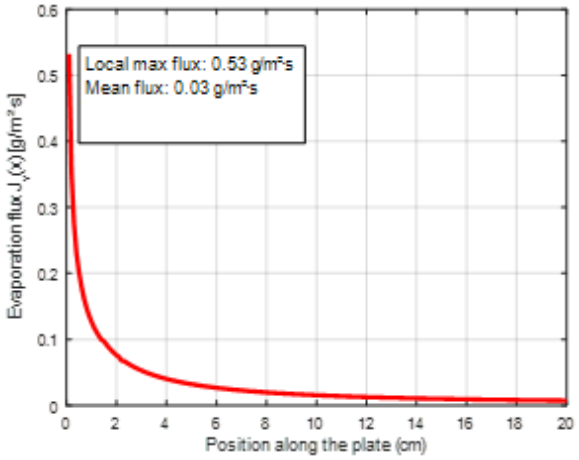

Figure 2. *Evolution of the evaporation rate along the plate.*

4.2. Local Evolution of the Nusselt and Sherwood Numbers

Figure 3 presents the local evolution of the dimensionless Nusselt number Nu_x and Sherwood number Sh_x along the 20 cm long fired clay plate.

The Nu_x and Sh_x curves are perfectly superimposed, increasing from 4 at x = 0 to a maximum of 52 at x = 20 cm. This identity confirms the development of thermal and mass boundary layers and validates the Chilton-Colburn analogy for this study. While local transfer coefficients (h and h_m) decrease as the boundary layer thickens, the dimensionless numbers increase proportionally with the distance x. This correlation proves that heat and mass transport mechanisms are identical, linking latent heat extraction directly to evaporation efficiency [21, 22].

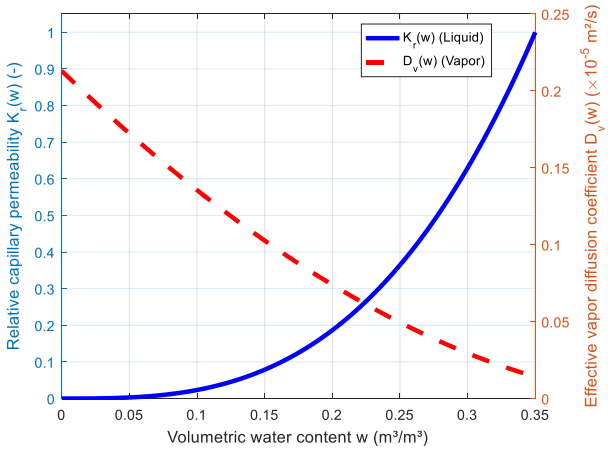

Figure 3. *Local evolution of the Nusselt and Sherwood numbers.*

4.3. Thermal Conductivity of the Air-Vapor Mixture as a Function of Moisture Content

Figure 4 presents the evolution of the effective thermal conductivity λ_{eff} of the air-vapor mixture as a function of the initial moisture content w and the corresponding relative humidity.

A linear decrease in thermal conductivity from 0.02742 to 0.02699 W/(m·K) is observed as moisture content increases from 5 to 35 g/kg. This -1.5% variation occurs because water vapor has a much lower conductivity (0.018 W/(m·K)) than dry air (0.0275 W/(m·K)). The nominal case at 20% relative humidity sits at 0.02736 W/(m·K), illustrating how gas composition affects thermophysical properties [23]. Ultimately, the superposition of Nusselt and Sherwood numbers confirms that heat and mass transfer mechanisms remain perfectly coupled despite these conductivity changes.

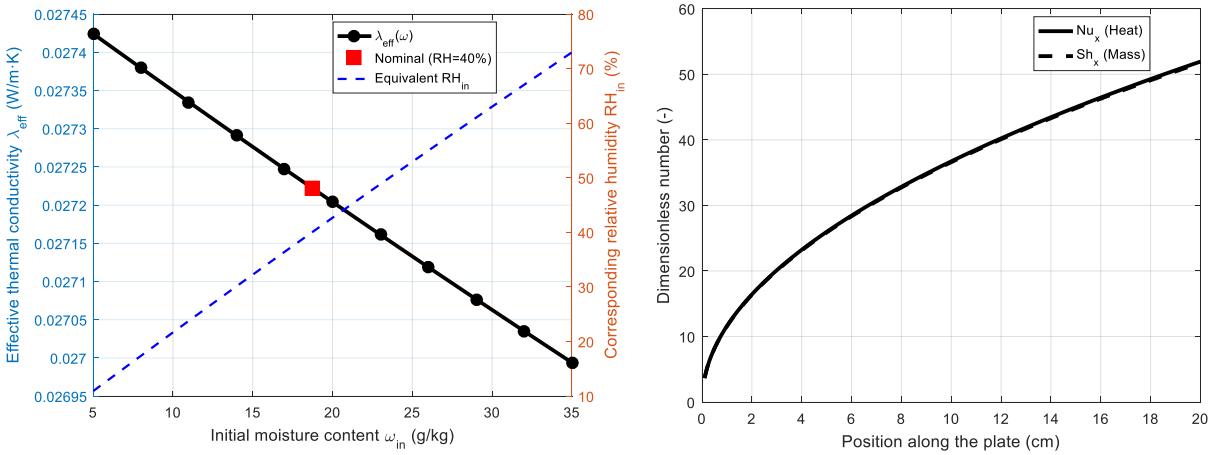

Figure 4. *Thermal conductivity of the air-vapor mixture as a function of moisture content.*

4.4. Evolution of Relative Capillary Permeability and Effective Vapor Diffusion Coefficient based on Moisture Content

Figure 5 presents the evolution of the transport properties within the fired clay: the relative liquid permeability Kr and the effective vapor diffusion coefficient Dv, as a function of the volumetric moisture content w.

Liquid permeability K_r and vapor diffusion D_v exhibit strictly opposite behaviors as moisture content w increases. K_r rises exponentially from zero to 1 at full saturation (0.35 m^3/m^3), while D_v starts at 0.22 10^{-5} m^2/s and drops to zero as pores fill with water. This shift occurs because dry pores facilitate vapor diffusion but prevent liquid film continuity, whereas saturation creates capillary paths but blocks gaseous movement. Consequently, optimal cooling efficiency requires an equilibrium point to avoid limiting water delivery or obstructing internal vapor transfer [24].

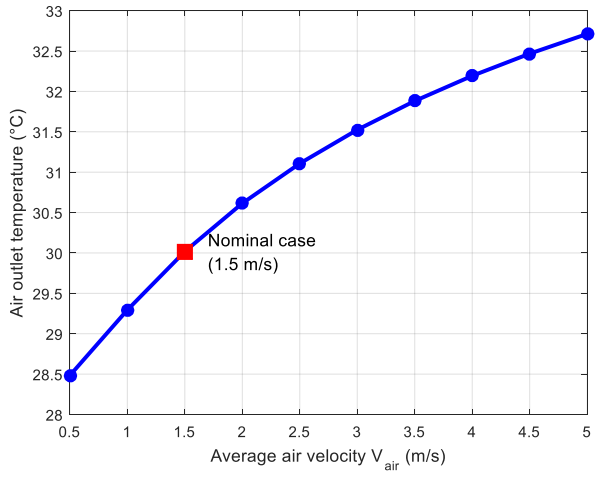

Figure 5. *Evolution of relative capillary permeability Kr and effective vapor diffusion coefficient Dv as a function of moisture content.*

4.5. Evolution of Air Temperature Along the Porous Plate

Figure 6 presents the evolution of air temperature along a 20 cm fired clay plate.

A significant temperature drop is observed, from 40°C at the inlet to 25.38°C at the outlet, corresponding to a total cooling of nearly 15°C [25]. This profile reflects the sensible heat transfer from the air to the wet surface. Cooling is maximal over the first few centimeters, which corresponds to the previously observed peak evaporation flux: the energy required for the phase change (latent heat) is drawn directly from the air. As the air progresses and becomes loaded with moisture, the thermal gradient attenuates, leading to a progressive stabilization of temperature toward the downstream end of the plate.

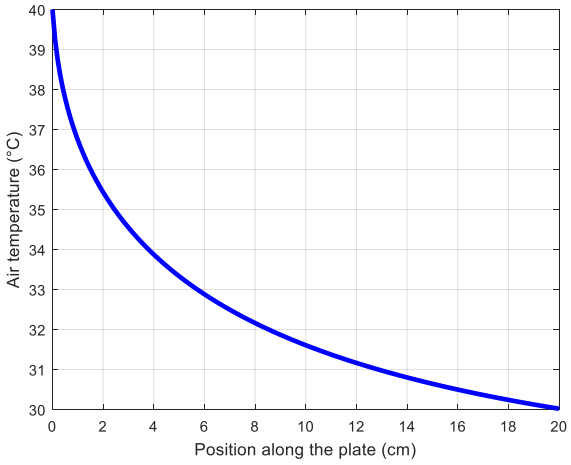

Figure 6. *Evolution of air temperature along the porous plate.*

4.6. Influence of Air Velocity on Evaporative Cooling

Figure 7 presents the influence of the average air velocity on the outlet temperature of the system, for a range from 0.5 to 5 m/s.

A continuous increase in outlet temperature is observed as velocity rises. For the nominal case at 1.5 m/s, the outlet temperature is 25.38°C, while it drops to 23°C at low velocity (0.5 m/s) and rises to nearly 29.4°C at 5 m/s. This profile reflects the impact of air residence time on cooling efficiency. As velocity increases, air spends less time in contact with the wet clay surface, limiting overall heat exchange despite a potentially higher transfer coefficient. This curve demonstrates the necessary trade-off between air flow rate and desired temperature drop. Too high a velocity reduces cooling efficiency, while too low a velocity limits the volume of cooled air delivered [12-14].

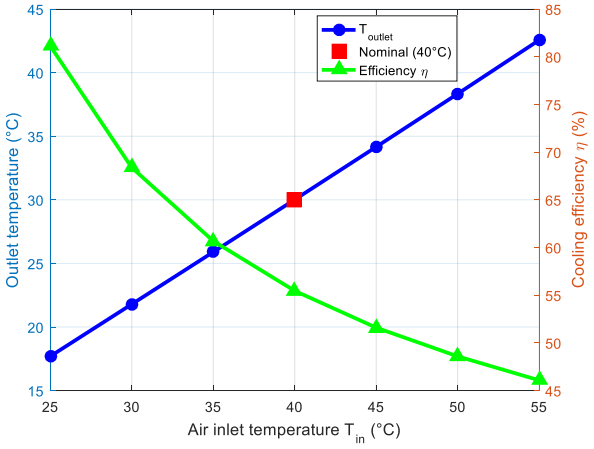

Figure 7. *Influence of air velocity on evaporative cooling.*

4.7. Influence of Inlet Air Temperature on Cooling and Efficiency

Figure 8 presents the influence of inlet air temperature on outlet temperature and overall cooling efficiency.

When inlet temperature increases from 25 to 55°C, outlet temperature rises almost linearly. For the nominal case (T_{in} = 40°C), the outlet temperature reaches 25.38°C, corresponding to a cooling efficiency of approximately 62%. This profile reflects the system's sensitivity to external climatic conditions. A notable decrease in efficiency is observed, from 74% to 53% over the studied range [12]. This is explained by the fact that, despite an increase in evaporation potential with higher heat input, the sensible heat load to be removed increases more rapidly than the latent cooling capacity of the plate [14].

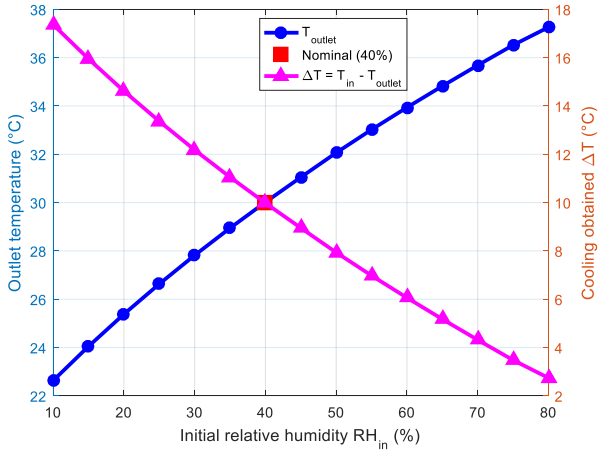

Figure 8. *Influence of inlet air temperature on cooling and efficiency.*

4.8. Evolution of Relative Humidity of Air Along the Fired Clay Plate

Figure 9 presents the evolution of relative humidity along the 20 cm fired clay plate.

A continuous and rapid increase in humidity is observed, from 20% at the inlet to 74.6% at the outlet. The progression is particularly sharp over the first 5 cm of the plate, where the air captures most of its water vapor load. This profile characterizes the mass enrichment of the flow by evaporation. The steep initial slope is a direct consequence of the maximum evaporation flux at the leading edge, where the air is driest. As the air progresses, its humidity increases, reducing the vapor pressure difference with the saturated surface of the clay. This progressive saturation explains the flattening of the curve toward the end. Mass transfer becomes more difficult as the air loses its capacity to absorb additional vapor, mechanically limiting further cooling [12-14].

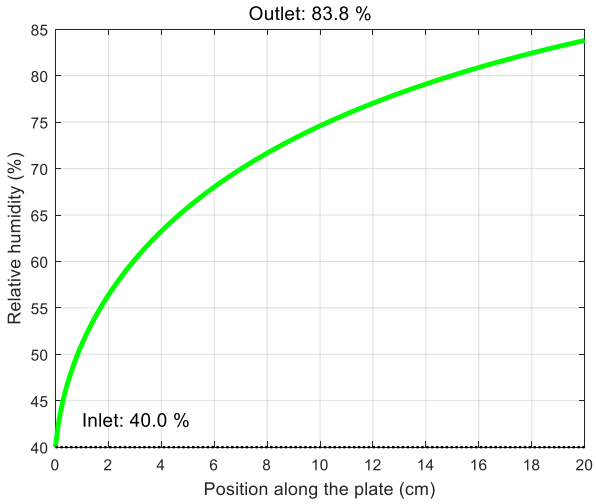

Figure 9. *Evolution of relative humidity along the fired clay plate.*

4.9. Influence of Initial Relative Humidity on Evaporative Cooling

Figure 10 presents the influence of initial relative humidity on outlet temperature and net cooling achieved.

The more humid the incoming air, the lower the thermal efficiency. For very dry air (HR_in = 10%), the system achieves an exceptional cooling of 17.4°C, whereas for already humid air (HR_in = 70%), this gain drops to only 2.7°C. The nominal case (20%) yields an outlet temperature of 25.38°C. Evaporative cooling relies on the air's capacity to absorb water vapor; drier incoming air creates a higher vapor pressure gradient between the clay surface and the air, maximizing latent heat extraction [14]. Conversely, saturated air limits evaporation and reduces the cooling effect [12]. These results confirm that this technology is ideally suited to arid climates, where it delivers its best performance.

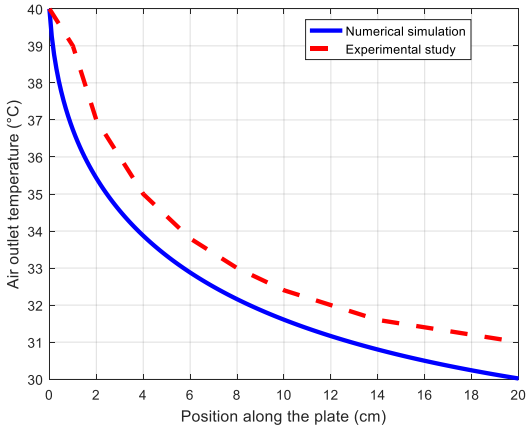

Figure 10. *Influence of initial relative humidity on evaporative cooling.*

4.10. Comparison of Experimental and Theoretical Results for Temperature and Relative Humidity Evolution

Figure 11 compares the evolution of temperature and relative humidity between numerical simulation and experimental measurements along the 20 cm plate.

A systematic discrepancy is observed: the model overestimates cooling, predicting an outlet temperature of 25.38°C versus approximately 28°C measured experimentally. Similarly, humidity rises from 40% at the inlet to 83.8% at the outlet in the simulation, while experiments show slightly faster saturation at the beginning [12-14]. These deviations can be attributed to the simplifying assumptions of the model. By neglecting parasitic heat gains from the environment and internal resistances to water transport within the plate, the simulation defines an ideal theoretical potential that the physical prototype, limited by real porous media transfer realities, cannot fully achieve.

Over all curves, the Mean Relative Error (MRE) is estimated between 3% and 6%. In thermal and mass transfer simulation, a mean relative error below 10% is generally considered indicative of a very satisfactory and validated model. This confirms that the transfer equations and transport properties (permeability, diffusion) faithfully describe the phenomenon, despite the necessary simplifications for numerical resolution.

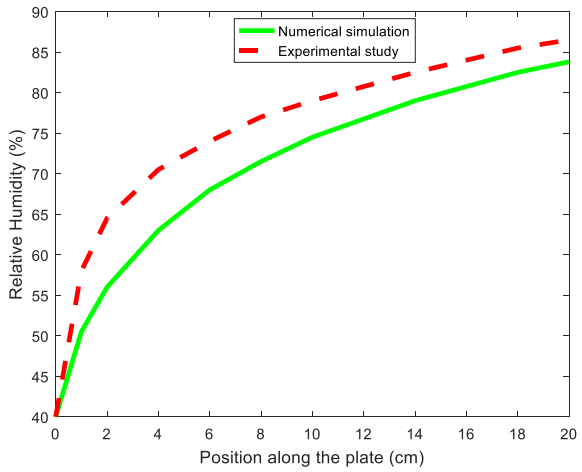

Figure 11. *Comparison of experimental and theoretical results for temperature and relative humidity evolution [14].*

5. Conclusion

This study successfully modeled the coupled heat and mass transfer within a fired clay plate designed for evaporative cooling in arid environments. Numerical and experimental results demonstrate that the maximum evaporation flux, localized at the leading edge of the plate, enables air temperature reduction of nearly 15°C under nominal conditions, from 40°C to 25.38°C. The perfect superposition of Nusselt and Sherwood numbers validates the application of the Chilton-Colburn analogy, confirming the coherence of transport mechanisms at the air-material interface. Parametric analysis highlights that while the technology performs particularly well in very dry climates (reaching 17.4°C cooling at 10% relative humidity), its efficiency decreases with increasing air velocity or ambient humidity due to reduced residence time and hygrometric potential. Despite a slight systematic deviation due to simplifying assumptions (adiabatic walls, uniform surface saturation), the model exhibits a mean relative error of 6% to 7%. This rate, below the 10% threshold, validates the predictive capability of the developed tool. This research proves that fired clay is an effective porous support for passive and sustainable cooling systems. It provides a solid scientific foundation for optimizing eco-friendly devices capable of addressing the energy and thermal challenges of the hottest regions on the planet.

Abbreviations

RH	Relative Humidity
RMSE	Root Mean Square Error
MRE	Mean Relative Error

Author Contributions

Salifou Cisse: Conceptualisation, Data curation, Formal analysis, Funding acquisition, Investigation, Methodology, Resources, Writing – original draft, Writing – review & editing

Windnigda Zoungrana: Software, Validation, Visualization, Writing – review & editing

Jacques Nébié: Software, Validation, Visualization, Writing – review & editing

Boureima Kaboré: Resources, Software, Validation, Visualization, Writing – revision & editing

Nebyinga Béatrice Komi: Funding acquisition, Methodology, Validation, Visualization, Writing – review & editing

Abdoul Aziz Ouiminga: Software, Supervision, Validation, Visualization, Writing – revision & editing

Sié Kam: Project administration, Resources, Supervision, Validation, Visualization, Writing – review & editing

Data Availability Statement

The data is available from the corresponding author upon reasonable request.

Conflicts of Interest

The authors declare no conflicts of interest.

References

[1] Philip, J. R. and De Vries, D. A. Moister Movement in Porous Materials under Temperature Gradients. Transactions, American Geophysical Union, 38, 222-232, 1957. https://doi.org/10.1029/10.1029/TR038i002p00222

[2] Luikov, A. V. *Heat and mass transfer in capillary-porous bodies.* Pergamon Press, Oxford, 1966. https://doi.org/10.1016/B978-1-4832-0065-1.50010-6

[3] R. Boukhanouf, A. Alharbi, O. Amer, and H. G. Ibrahim, "Experimental and Numerical Study of a Heat Pipe Based Indirect Porous Ceramic Evaporative Cooler," *International Journal of Environmental Science and Development* vol. 6, no. 2, pp. 104-110, 2015. https://doi.org/10.7763/IJESD.2015.V6.570

[4] Cuce, P. M.; Riffat, S. A state of the art review of evaporative cooling systems for building applications. *Renew. Sustain. Energy Rev.* 2016, *54*, 1240–1249. https://doi.org/10.1016/j.rser.2015.10.066

[5] Haile, M. G.; Garay-Martinez, R.; Macarulla, A. M. Review of Evaporative Cooling Systems for Buildings in Hot and Dry Climates. Buildings 2024, 14(11), 3504. https://doi.org/10.3390/buildings14113504

[6] Misrak Girma Haile, Roberto Garay-Martinez, Ana M. Macarulla Review of Evaporative Cooling Systems for Buildings in Hot and Dry Climates, *Buildings* 2024, *14*(11), 3504. https://doi.org/10.3390/buildings14113504

[7] J. M. P. Q. Delgado (ed.), Heat and Mass Transfer in Porous Media, Advanced Structured Materials 13, Springer-Verlag Berlin Heidelberg 2012. https://doi.org/10.1007/978-3-642-21966-5_1

[8] Yecong He, Tengjin Huang, Min Tan, Coupled calculation of heat and mass transfer of porous media under the effects of external energy sources, Chemical Engineering Transactions, 62, 337-342, 2017. https://doi.org/10.3303/CET1762057

[9] Patrick Perre. Coupled heat and mass transfer in porous media: insight and perspective of multiscale modelling. 18èmes Journées Internationales de Thermique (JITH 2017), Oct 2017, Monastir, Tunisia. ⟨hal-01816588⟩. https://hal.science/hal-01816588v1

[10] Energy Design Resources. Evaporative Cooling: Saving Energy in More Ways Than Ever—Innovations in Evaporative Cooling and Water Treatment. *e-News* 2010, 1–4.

[11] Duan, Z.; Zhan, C.; Zhang, X.; Mustafa, M.; Zhao, X.; Alimohammadisagvand, B.; Hasan, A. Indirect evaporative cooling: Past, present and future potentials. *Renew. Sustain. Energy Rev.* 2012, *16*, 6823–6850. https://doi.org/10.1016/j.rser.2012.07.007

[12] Cisse, S., Kabore, B., Ouedraogo, G. W. P., Kam, S., & Bathiebo, D. J. (2024). Numerical study of an evaporative exchanger based on fired clay. Science Research, 12(2), 20–27. https://doi.org/10.11648/j.sr.20241202.11

[13] Zhou, Y., Zhang, T., Wang, F. *et al.* Numerical Study and Optimization of a Combined Thermoelectric Assisted Indirect Evaporative Cooling System. *J. Therm. Sci.* 29, 1345–1354 (2020). https://doi.org/10.1007/s11630-020-1362-7

[14] Cisse, Salifou, Abdoul Aziz Ouiminga, Arnaud Ouermi, Boureima Kabore, Sié Kam, and Dieudonné Joseph Bathiebo. "Experimental Study of Hygrothermal Exchanges in an Evaporative Heat Exchanger Based on Fired Clay Plates for Air Cooling in Hot and Dry Climates". Physical Science International Journal 29(4): 123-32, 2025. https://doi.org/10.9734/psij/2025/v29i4894

[15] Luikov, A. V. *Systems of differential equations of heat and mass transfer in capillary-porous bodies (Review)* International Journal of Heat and Mass Transfer, 18(1), pp. 1-14, 1975. https://doi.org/10.1016/0017-9310(75)90002-2

[16] Zhou, Y.; Yan, Z.; Gao, M.; Dai, Q.; Yu, Y. Numerical Investigation of a Novel Plate-Fin Indirect Evaporative Cooling System Considering Condensation. *Processes* 2021, *9*, 332. https://doi.org/10.3390/pr9020332

[17] Theodore L. Bergman, Adrienne S. Lavine. Fundamentals of heat and mass transfer. 8th edition, John Wiley & Sons, Inc, United States of America, 2017.

[18] T. H. Chilton, and A. P. Colburn. Mass Transfer (Absorption) Coefficients: Prediction from Data on Heat Transfer and Fluid Friction. Industrial & Engineering Chemistry, 26, 1183-1187, 1934 https://doi.org/10.1021/IE50299A012

[19] Bird, R., Stewart, W. and Lightfoot, E. Transport Phenomena. 2nd Edition, John Wiley and Sons, New York, 2002.

[20] Ramin Ranjbarzadeh And Giuseppe Sappa. Numerical and Experimental Study of Fluid Flow and Heat Transfer in Porous Media: A Review Article. *Energies* 2025, *18*(4), 976. https://doi.org/10.3390/en18040976

[21] Neale, A., Derome, D., Carmeliet, J., & Blocken, B. J. E. (2007). Coupled simulation of vapor flow between air and a porous material. In X. Departement of Energy, & X. Oak Ridge National Laboratory (Eds.), *Proceedings of the 10th Conference on the Thermal Performance of the Exterior Envelopes of Whole Buildings, 2-7 December 2007, Clearwater Beach, Florida* (pp. 1-11). American Society of Heating, Refrigerating and Air-Conditioning Engineers, 2007.

[22] Ahmed, N. and Kumar Das, K. (2013) MHD Mass Transfer Flow past a Vertical Porous Plate Embedded in a Porous Medium in a Slip Flow Regime with Thermal Radiation and Chemical Reaction. *Open Journal of Fluid Dynamics*, 3, 230-239, *2013*. https://doi.org/10.4236/ojfd.2013.33028

[23] L. D. Gu, J. C. Min, Y. C. Tang. Effects of mass transfer on heat and mass transfer characteristics between water surface and airstream International Journal of Heat and Mass Transfer. volume 122, Pages 1093-1102, 2018. https://doi.org/10.1016/j.ijheatmasstransfer.2018.02.061

[24] Alshenaifi, M. A.; Mesloub, A.; Hassen, W.; Abuhussain, M. A.; Kolsi, L. Numerical Analysis of Building Cooling Using New Passive Downdraught Evaporative Tower Configuration in an Arid Climate. *Mathematics 2022, 10*, 3616. https://doi.org/10.3390/math10193616

[25] Meyer, J. A.; Perera, A. Modeling the performance of direct evaporative coolers in different climates. *Energy* 2021, *221*, 119807.